PRAMANA — journal of physics

Vol. 83, No. 5
November 2014
pp. 695–704

Density content of nuclear symmetry energy from nuclear observables

B K AGRAWAL
Saha Institute of Nuclear Physics, 1/AF Bidhan Nagar, Kolkata 700 064, India
E-mail: bijay.agrawal@saha.ac.in

DOI: 10.1007/s12043-014-0856-9; ***e*Publication:** 11 October 2014

Abstract. The nuclear symmetry energy at a given density measures the energy transferred in converting symmetric nuclear matter into the pure neutron matter. The density content of nuclear symmetry energy remains poorly constrained. Our recent results for the density content of the nuclear symmetry energy, around the saturation density, extracted using experimental data for accurately known nuclear masses, giant resonances and neutron-skin thickness in heavy nuclei are summarized.

Keywords. Symmetry energy parameters; nuclear matter; neutron skin.

PACS Nos 21.65.Ef; 21.65.Mn; 21.10.Gv

1. Introduction

The study of symmetry energy is currently a subject of great interest. Most of the stable nuclei, except for the light nuclei with proton number $Z \leq 28$, are asymmetric. The accurate knowledge of the nuclear symmetry energy and its density dependence would play extremely important roles in the study of the structure of finite nuclei. The matter in the neutron stars are also asymmetric. The asymmetry arises due to the requirements that the matter in the neutron stars must be charge neutral and in β-equilibrium. Such matter is highly asymmetric, it is predominantly composed of neutrons and so the symmetry energy critically controls the nuclear pressure of such a system.

The nuclear part of the equation of state (EoS) for the neutron star matter can be approximately written as

$$\epsilon(\rho, I) = \epsilon(\rho, 0) + J(\rho)I^2 + \cdots, \tag{1}$$

where $\epsilon(\rho, I)$ is the energy per nucleon, $\rho = \rho_n + \rho_p$, $I = (\rho_n - \rho_p)/\rho$ is the asymmetry with ρ_n and ρ_p being densities of the neutrons and the protons. The symmetry energy

coefficient $J(\rho)$ can be expressed in terms of the various symmetry energy parameters evaluated at the saturation density ρ_0 as

$$J(\rho) = J(\rho_0) + L(\rho_0)\left(\frac{\rho-\rho_0}{3\rho_0}\right) + \frac{1}{2}K_{\rm sym}(\rho_0)\left(\frac{\rho-\rho_0}{3\rho_0}\right)^2. \tag{2}$$

The symmetry energy J, slope L and curvature $K_{\rm sym}$ can be evaluated as

$$J(\rho) = \frac{1}{2}\left.\frac{{\rm d}^2\epsilon(\rho, I)}{{\rm d}I^2}\right|_{I=0}, \tag{3}$$

$$L(\rho_0) = 3\rho_0\left.\frac{{\rm d}J(\rho)}{{\rm d}\rho}\right|_{\rho=\rho_0}, \tag{4}$$

$$K_{\rm sym}(\rho_0) = 9\rho_0^2\left.\frac{{\rm d}^2J(\rho)}{{\rm d}\rho^2}\right|_{\rho=\rho_0}, \tag{5}$$

Particular attention is given to constrain, in a narrow window, the value of L at the nuclear matter saturation density $\rho_0 = 0.16$ fm^{-3}. The value of L at ρ_0 affects the nuclear binding energies and the nuclear drip lines and has a crucial role in determining the neutron density distribution in neutron-rich nuclei. The high-density behaviour of the EoS for the neutron star matter is also governed by the values of L at supranormal densities ($\rho \gg \rho_0$).

The symmetry energy is not a directly measurable quantity. It has to be extracted indirectly from various observables. One needs accurate knowledge of the large variety of phenomena in order to map the nuclear symmetry energy over a wide range of density. The nuclear multifragmentation and cluster formation at low densities probe the nuclear symmetry energy at the subsaturation densities ($\rho < \rho_0$) [1,2]. The symmetry energy close to the nuclear saturation density can be probed by the neutron-skin thickness and the isovector giant dipole resonances in heavy nucleus like ^{208}Pb [3]. The high-density behaviour of the symmetry energy can be understood in terms of various observables associated with the neutron stars [4]. In this paper, we shall summarize some of the recent results of $L(\rho_0)$ extracted using the data for various nuclear observables.

2. $L(\rho_0)$ from the nuclear observables

The nuclear observables considered are: (i) neutron-skin thickness in ^{208}Pb nucleus, (ii) giant resonances in ^{208}Pb nucleus and (iii) nuclear masses. In what follows, we briefly summarize the current status of $L(\rho_0)$ derived on the basis of the knowledge of these observables.

2.1 *Neutron-skin thickness*

The value in $L(\rho_0)$ has been shown [5] to be strongly correlated with the neutron-skin thickness in ^{208}Pb nucleus. The neutron-skin thickness denoted as $R_{\rm skin}$ is defined as

the difference between the neutron and proton root mean square (r.m.s.) radii. The correlation of $L(\rho_0)$ with $R_{\rm skin}$ suggests that tight bounds on $L(\rho_0)$ requires knowledge of $R_{\rm skin}$ to be accurate within 0.5%. To illustrate, in figure 1 we plot the variation of $L(\rho_0)$ with neutron-skin thickness in ^{208}Pb nucleus obtained for two different families of the relativistic mean-field (RMF) models, namely FSU-V and TM1*-V. These two different families are obtained by systematically varying the parameters of the commonly used FSU and the TM1* models. One may notice that $R_{\rm skin}$ is well-correlated with $L(\rho_0)$ within a given family. Marginal model dependence however exists in the $L(\rho_0) - R_{\rm skin}$ correlation which might arise due to the differences in the functional forms of the Lagrangian densities associated with these models. The information content of neutron-skin thickness based on covariance analysis [6] once again yields a strong correlation between $R_{\rm skin}$ and $L(\rho_0)$. The lead radius experiment (PREX) [7,8] has recently measured $R_{\rm skin}$ of ^{208}Pb. This experiment was performed via parity-violating electron scattering [9] and provide the first purely electroweak, model-independent, measurement of the neutron distribution of a heavy nucleus. By measuring the neutron form factor of ^{208}Pb at momentum transfer $q \approx 0.475$ fm^{-1}, PREX was able to determine $R_{\rm skin} = 0.33^{+0.16}_{-0.18}$ fm [8]. Alternatively, hadronic probes are used to estimate the neutron distribution in the nuclei. However, these probes are model-dependent and display large theoretical uncertainties. The analysis from recent experiments have led to varying values of the neutron-skin thickness, $R_{\rm skin} = 0.16 \pm 0.02$(stat.)$\pm 0.04$(syst.) fm and $R_{\rm skin} = 0.211^{+0.054}_{-0.063}$ fm. The accurate and model-independent value for $R_{\rm skin}$ is still awaited.

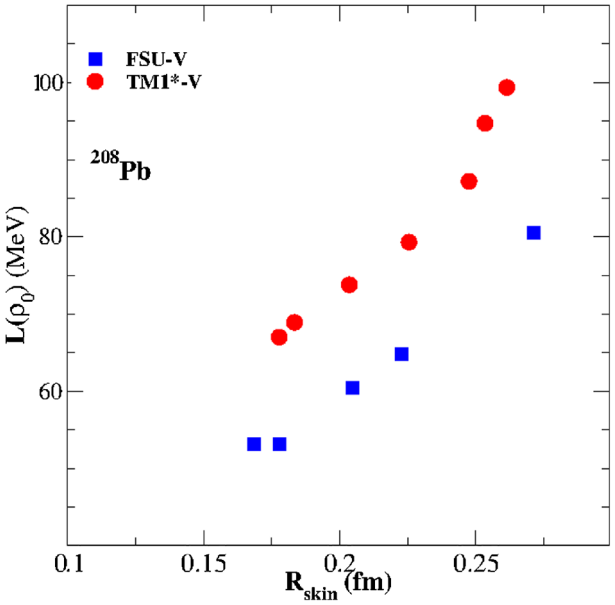

Figure 1. The variations of the symmetry energy slope parameter $L(\rho_0)$ with the neutron-skin thickness $R_{\rm skin}$ for the systematically varied FSU and TM1* models.

2.2 *Giant resonance*

Nuclear dipole polarizibility α_D, related to the inverse energy weighted sum rule for the isovector giant dipole resonance, has been suggested [6,10] as an alternative observable constraining the neutron skin. The recent high-resolution (p, p') measurement [11] of α_D together with the results of the covariance analysis based on single model gives the neutron-skin thickness of ^{208}Pb to be $0.156^{+0.025}_{-0.021}$ fm. In ref. [3], we have investigated the model dependance of correlations between α_D and R_{skin} in ^{208}Pb using different types of nuclear energy density functionals. The α_D and R_{skin} correlations were found to be strong within the individual family of models. The results obtained by combining the different families of models yielded relatively weaker α_D–R_{skin} correlations which shifted the value of R_{skin} to 0.168±0.022 fm. These values of R_{skin} gave rise to $L(\rho_0) = 47 \pm 12$ MeV.

The available data for the giant quadrupole resonance in ^{208}Pb also have been exploited to extract the values for R_{skin} and $L(\rho_0)$. It has been shown that excitation energy (E_x^{IV}) for the isovector giant quadrupole resonance depends on the effective nucleon mass as well as the density dependence of the symmetry energy, whereas, it is well known that the excitation energy (E_x^{IS}) for the isoscalar quadrupole resonance depends mainly on the effective nucleon mass. Based on the macroscopic model, it is realized that appropriate linear combination of the square of the isoscalar and isovector giant quadrupole resonance energies may be directly related to R_{skin} [12]. In figure 2, the values of $((E_x^{IV})^2 - 2(E_x^{IS})^2)/J$ are plotted as a function of R_{skin} for ^{208}Pb nucleus. The shaded region depicts the experimental data for $((E_x^{IV})^2 - 2(E_x^{IS})^2)/J$ obtained using the values for $E_x^{IV} = 22.7 \pm 0.2$ MeV and $E_x^{IS} = 10.9 \pm 0.1$ MeV and the value $J = 32 \pm 1$ MeV. As a result $R_{skin} = 0.15 \pm 0.02$ fm which leads to $L(\rho_0) = 31 \pm 10$ MeV.

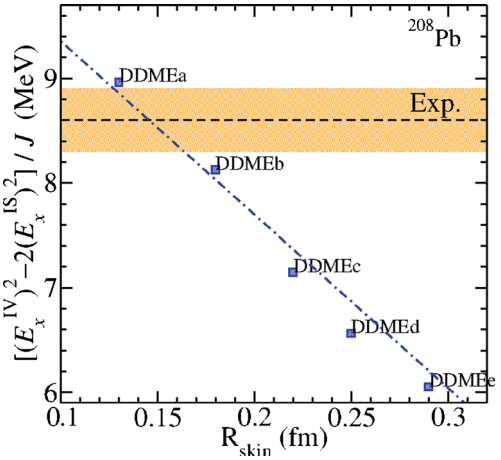

Figure 2. Values of $((E_x^{IV})^2 - 2(E_x^{IS})^2)/J$ as functions of R_{skin} in ^{208}Pb, calculated with the density-dependent meson exchange DDME models. The dashed line with shaded band indicates the experimental value and the corresponding uncertainty.

2.3 *Nuclear masses*

The precise data on the nuclear masses for a large number of nuclei enable one to determine the values of the volume and surface symmetry energy coefficients within small uncertainties. We present here some of the recent results [13,14] for the values of $L(\rho_0)$ and $R_{\rm skin}$ of ^{208}Pb extracted using empirical values of the volume symmetry energy and the surface symmetry energy coefficient [15].

The symmetry energy coefficient, $a_{\rm sym}(A)$, for a nucleus with mass number A can be expressed in terms of $J(\rho_0)$ and $J_{\rm s}$ as

$$a_{\rm sym}(A) = J(\rho_0) - J_{\rm s}A^{-1/3}, \tag{6}$$

where J and $J_{\rm s}$ are the volume and surface symmetry energy coefficients, respectively. A meticulous study [15] of the double differences of 'experimental' symmetry energies were done in the recent past. The double differences in symmetry energies of the neighbouring nuclei has the advantage that effects from pairing and shell corrections are cancelled out well, resulting in a compact correlation between the double differences and the mass number of the nuclei. This yields values of $J(\rho_0)$ and $J_{\rm s}$ as 32.1±0.31 MeV and 58.91 ±1.08 MeV, respectively. The uncertainties in $J(\rho_0)$ and $J_{\rm s}$ are much smaller than those found previously.

For a finite nucleus of mass number A, the symmetry coefficient $a_{\rm sym}(A)$ is always less than $J(\rho_0)$. The coefficient $a_{\rm sym}(A)$ can be equated to $J(\rho_A)$ [5], where ρ_A is an equivalent density, always less than ρ_0. Thus, by using eq. (6),

$$J(\rho_A) = J(\rho_0) - J_{\rm s}A^{-1/3}. \tag{7}$$

The left-hand side of the above equation can be expanded around the density ρ_0 as

$$J(\rho_A) = J(\rho_0) - L\epsilon_A + \frac{K_{\rm sym}}{2}\epsilon_A^2, \tag{8}$$

where

$$K_{\rm sym} = 9\rho^2\frac{{\rm d}^2J(\rho)}{{\rm d}\rho^2}\bigg|_{\rho_0} \quad \text{and} \quad \epsilon_A = (\rho_0 - \rho_A)/3\rho_0. \tag{9}$$

Combining eqs (7) and (8) we get

$$J_{\rm s} = A^{1/3}\left[L\epsilon_A - \frac{K_{\rm sym}}{2}\epsilon_A^2\right]. \tag{10}$$

The value of symmetry coefficient $a_{\rm sym}(A)$ or equivalently $J(\rho_A)$ can also be calculated in the local density approximation as [16]

$$J(\rho_A) = \frac{1}{AX_0^2}\int {\rm d}^3r\rho(r)J(\rho(r))[X(r)]^2, \tag{11}$$

where X_0 is the isospin asymmetry (= $(N-Z)/A$) of the nucleus, $\rho(r)$ is the sum of the neutron and proton densities inside the nucleus and $X(r)$ is the local isospin asymmetry.

We start with the ansatz

$$J(\rho) = J(\rho_0)\left(\frac{\rho}{\rho_0}\right)^{\gamma}, \tag{12}$$

where γ measures the density dependence of the symmetry energy. In a considerable density range around ρ_0, this ansatz is found to be very consistent with the density dependence obtained from the nuclear EoS with different interactions [1,16,17] and also from experiments in intermediate-energy heavy-ion collisions [2,18]. From eqs (4) and (9) we get

$$L = 3\gamma J(\rho_0) \tag{13}$$

and

$$K_{\rm sym} = 9\gamma(\gamma - 1)J(\rho_0). \tag{14}$$

We obtain using eqs (10–14)

$$J_{\rm s} = 3\gamma\epsilon_A J(\rho_0)A^{1/3}\left[1 - \frac{3}{2}(\gamma - 1)\epsilon_A\right] \tag{15}$$

and

$$(\rho_A)^\gamma = \frac{1}{AX_0^2}\int {\rm d}^3 r\,\rho(r)^{\gamma+1}[X(r)]^2. \tag{16}$$

Given the neutron–proton density profiles in the nucleus, from eq. (16), a chosen value of γ gives ρ_A and hence ϵ_A. The one that satisfies eq. (15) for the given empirical values of

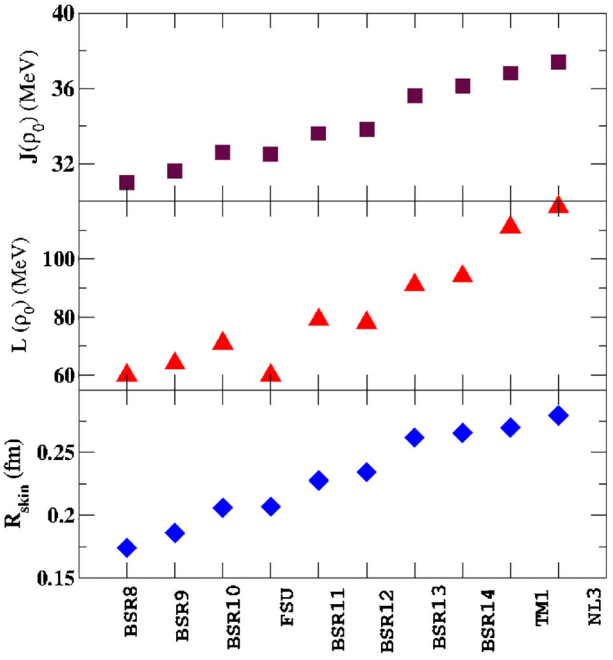

Figure 3. The values of volume symmetry energy coefficient $J(\rho_0)$, slope parameter $L(\rho_0)$ and the neutron-skin thickness for the ^{208}Pb nucleus for different parametrizations of the selected RMF models.

$J(\rho_0)$, J_s and ρ_0 is the desired solution for γ. Once γ is known, the equivalent density ρ_A, the symmetry energy slope parameter and symmetry incompressibility are determined. The neutron and proton density profiles are obtained within the RMF models. These models are so chosen that they yield the experimental proton r.m.s. radius but varying neutron-skin thickness for the ^{208}Pb nucleus. The parameters of the interactions BSR8-BSR14 [19], FSUGOLD [20], NL3 [21] and TM1 [22] have been used to generate the proton and neutron density profiles of ^{208}Pb in the RMF model. In figure 3 we display the values of $J(\rho_0)$, $L(\rho_0)$ and $R_{\rm skin}$ for the ^{208}Pb nucleus obtained for these different parametrizations of the RMF model.

Ansatz for $J(\rho)$, different from that given by eq. (7) but consistent with the density dependence obtained from the nuclear EoS with different interactions can also be chosen. As long as the functional form for $J(\rho)$ depends only on a single parameter, expressions analogous to eqs (15) and (16) can be obtained. We have considered a different functional form for $J(\rho)$ in addition to that of eq. (12) in order to check the robustness of our results. We use

$$J(\rho) = c_k \left(\frac{\rho}{\rho_0}\right)^{2/3} + c_1 \left(\frac{\rho}{\rho_0}\right) + c_2 \left(\frac{\rho}{\rho_0}\right)^{5/3}, \tag{17}$$

where

$$c_k = (2^{2/3} - 1)\frac{5}{3}\frac{P_{\rm F,0}^2}{2m^*} \tag{18}$$

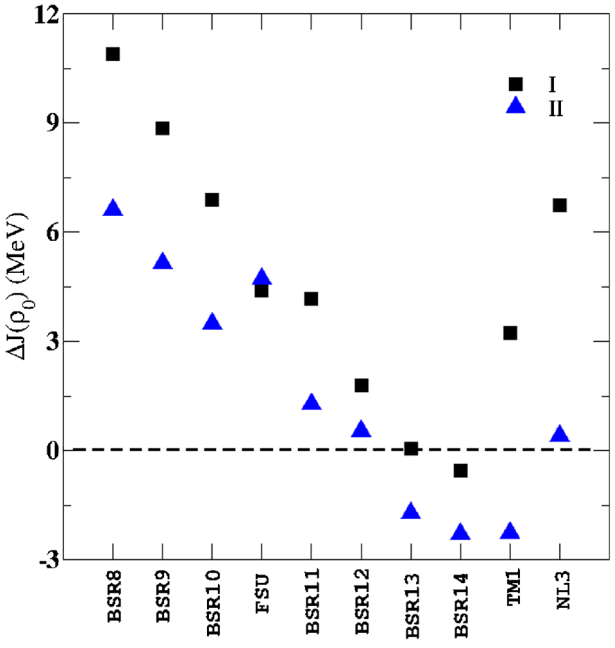

Figure 4. The error $\Delta J(\rho_0)$ calculated at ρ_0 are shown for the various interactions pertaining to Cases I and II.

is the kinetic energy contribution to the symmetry energy coefficient and

$$c_2 = J(\rho_0) - c_1 - c_k \tag{19}$$

with $P_{\mathrm{F},0}$ being the Fermi momentum corresponding to the saturation density ρ_0 and m^* is the nucleon effective mass. The functional form for $J(\rho)$ given by eq. (17) has been employed recently in [23] to validate the relationship between J, L and K_{sym} at ρ_0. Hereafter, the different functional forms for $J(\rho)$, given by eqs (12) and (17), will be referred to as Cases I and II, respectively. These cases yield the relations between $J(\rho_0)$, L and K_{sym} at density ρ_0 which are as follows:

$$J(\rho_0) = \frac{L}{3 + K_{\mathrm{sym}}/L} \tag{20}$$

and

$$J(\rho_0) = \frac{L}{3} - \frac{K_{\mathrm{sym}}}{15} + \frac{c_k}{5}. \tag{21}$$

The results for the error $\Delta J(\rho_0)$, obtained using different RMF models, are displayed in figure 4. $\Delta J(\rho_0)$ is the difference between the exact value of $J(\rho_0)$ and the one calculated using the right-hand side of eqs (20) and (21). The departure of $\Delta J(\rho_0)$ from zero is indicative of the inaccuracy involved in expressing the functional dependence of

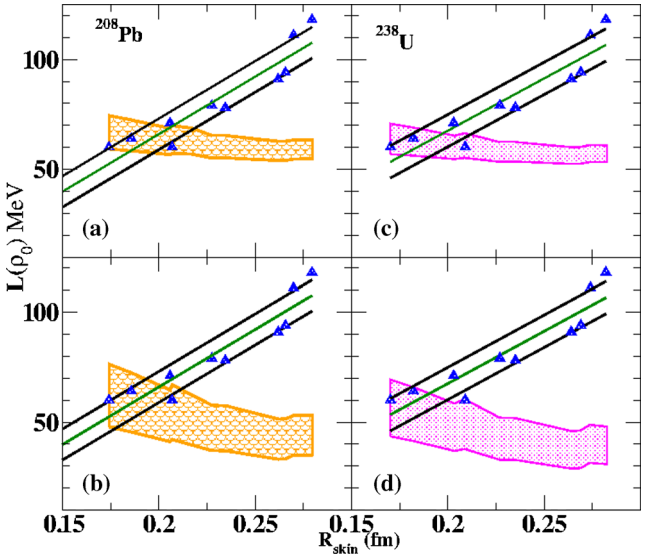

Figure 5. The symmetry energy slope parameter L calculated using eq. (4) plotted as a function of R_{skin} of ^{208}Pb and ^{238}U evaluated with different RMF interactions are shown by the blue triangles. The green lines with envelopes of slanted black lines refer to the least-squared fits to them with the spread-out error. The shaded regions in the (**a**, **b**) and (**c**, **d**) panels represent the envelope of possible L values calculated in Cases I and II. The acceptable range for values of L and R_{skin} are obtained from the intersection of the slanted envelopes and the shaded regions.

symmetry energy. The values of $\Delta J(\rho_0)$ for Case II (blue triangles) are quite similar for the interactions we have chosen; they lie closer to zero in comparison to those in Case I, except for the BSR13 and BSR14 interactions.

In figure 5, we display variations of the symmetry energy slope parameter L as a function of $R_{\rm skin}$ for ^{208}Pb and ^{238}U for Cases I and II. $R_{\rm skin}$ values are calculated using the density profiles for protons and neutrons obtained for various RMF interactions. The values of L for the blue filled triangle are obtained using eq. (4). Typically, almost linear correlations between L and $R_{\rm skin}$ exists. The green straight lines passing through the triangles are obtained by a least-squares fit. The thick black lines are drawn by taking into account the r.m.s. error in L due to deviations from the linear correlations between L and $R_{\rm skin}$. We also calculate L using the different functional forms for $J(\rho_0)$ as given by eqs (12) and (17) referred to as Cases I and II. The orange shaded region is obtained by using the empirical values for $J(\rho_0)$ ($= 32.1 \pm 0.31$ MeV), $J_{\rm s}$ ($= 58.91 \pm 1.08$ MeV) and ρ_0 ($= 0.155 \pm 0.008$ fm^{-3}). These values display totally different type of correlation of L with $R_{\rm skin}$, the weak dependence coming from the imposed empirical constraints. This different behaviour of L with $R_{\rm skin}$, shown by orange-shaded region, stems from the fact that the values of L are calculated by keeping $J(\rho_0)$ and $J_{\rm s}$ fixed. However, bulk properties of the finite nuclei yield strong correlations of L with $J(\rho_0)$ and $J_{\rm s}$. The overlap of thick black lines with the orange-shaded region projects out simultaneously, the acceptable values of neutron-skin thickness and the density slope parameter L. By combining the results for Cases I and II, we get the acceptable value of $L = 59 \pm 13$ MeV and $R_{\rm skin} = 0.196 \pm 0.021$ fm for ^{208}Pb nucleus.

3. Conclusions

Some of the recent estimates for the symmetry energy slope parameter L are presented. The values of L at the saturation density are determined from its correlations with the neutron-skin thickness and various quantities associated with giant dipole and quadrupole resonances in ^{208}Pb nucleus. The investigations based on the different families of the mean-field models indicate that highly accurate values of neutron-skin thickness is required to constrain L. Such accurate values of neutron-skin thickness, however, are not yet measured. The isovector giant dipole and quadrupole resonances yield the neutron-skin thickness in ^{208}Pb to be 0.17 ± 0.02 fm and 0.15 ± 0.02 fm which in turn leads to $L = 47 \pm 12$ MeV and 31 ± 10 MeV, respectively. It is also shown that, the values of L and the neutron-skin thickness in ^{208}Pb nucleus can be constrained simultaneously in a narrow window using empirical data for the volume and surface symmetry energies which are determined from the precisely known nuclear masses.

References

[1] B-A Li, L-W Chen and C M Ko, *Phys. Rep.* **464**, 113 (2008)
[2] M A Famiano *et al, Phys. Rev. Lett.* **97**, 052701 (2006)
[3] J Piekarewicz, B K Agrawal, G Colo, W Nazarewicz, N Paar, P-G Reinhard, X Roca-Maza and D Vretenar, *Phys. Rev. C* **85**, 024301 (2012)
[4] A W Steiner and Gandolfi, *Phys. Rev. Lett.* **108**, 081102 (2012)

[5] M Centelles, X Roca-Maza, X Vias and M Warda, *Phys. Rev. Lett.* **102**, 122502 (2009)
[6] P-G Reinhard and W Nazarewicz, *Phys. Rev. C* **81**, 051303 (2010)
[7] C J Horowitz, S J Pollock, P A Souder and R Michaels, *Phys. Rev. C* **63**, 025501 (2001)
[8] S Abrahamyan *et al*, *Phys. Rev. Lett.* **108**, 112502 (2012)
[9] J D Donnelly and I Sick, *Nucl. Phys. A* **503**, 589 (1989)
[10] J Piekarewicz, *Phys. Rev. C* **83**, 034319 (2011)
[11] A Tamii *et al*, *Phys. Rev. Lett.* **107**, 062502 (2011)
[12] X Roca-Maza, M Brenna, B K Agrawal, P F Bortignon, G Colò, L.-G. Cao, N Paar and D Vretenar, *Phys. Rev. C* **88**, 034301 (2013)
[13] B K Agrawal, J N De and S K Samaddar, *Phys. Rev. Lett.* **109**, 262501 (2012)
[14] B K Agrawal, J N De, S K Samaddaar, G Colo and A Sulaksono, *Phys. Rev. C* **87**, 051306(R) (2013)
[15] Y M Z H Jiang, G J Fu and A Arima, *Phys. Rev. C* **85**, 2012 (2012)
[16] S K Samaddar, J N De, X Vinas and M Centelles, *Phys. Rev. C* **76**, 041602(R) (2007)
[17] L-W Chen, C M Ko and B-A Li, *Phys. Rev. Lett.* **94**, 032701 (2005)
[18] D V Shetty, S J Yennello and G A Souliotis, *Phys. Rev. C* **76**, 024606 (2007)
[19] S K Dhiman, R Kumar and B K Agrawal, *Phys. Rev. C* **76**, 045801 (2007)
[20] B G Todd-Rutel and J Piekarewicz, *Phys. Rev. Lett.* **95**, 122501 (2005)
[21] G A Lalazissis, J Konig and P Ring, *Phys. Rev. C* **55**, 540 (1997)
[22] Y Sugahara and H Toki, *Nucl. Phys. A* **579**, 557 (1994)
[23] J Dong, W Zuo, J Gu and U Lombardo, *Phys. Rev. C* **85**, 034308 (2012)